TITLE

Strategic predatory pursuit of the stealthy, highly maneuverable, slow flying bat *Corynorhinus townsendii*

AUTHORS AND ROLES

Alberto Bortoni* (1), Sharon M. Swartz (1,2), Hamid Vejdani (3), Aaron J. Corcoran (4)

1. Department of Ecology, Evolution, and Organismal Biology, Brown University, Providence, RI 02912, USA.
2. School of Engineering, Brown University, Providence, RI 02912, USA.
3. Mechanical, Robotics, and Industrial Engineering, Lawrence Technological University, Southfield, MI 48075, USA.
4. Department of Biology, University of Colorado, Colorado Springs, CO 80918, USA.

*Correspondence: alb.bortoni@pm.me

KEYWORDS (3-6)

Pursuit; predation; guidance; predator-prey interaction.

ABSTRACT

A predator's capacity to catch prey depends on its ability to navigate its environment in response to prey movements or escape behavior. In predator-prey interactions that involve an active chase, pursuit behavior can be studied as the collection of rules that dictate how a predator should steer to capture prey. It remains unclear how variable this behavior is within and across species since most studies have detailed the pursuit behavior of high-speed, open-area foragers. In this study we analyze the pursuit behavior in 44 successful captures by *Corynorhinus townsendii*, Townsend's big-eared bat (n = 4). This species forages close to vegetation using slow and highly maneuverable flight, which contrasts with the locomotor capabilities and feeding ecologies of other taxa studied to date. Our results indicate that this species relies on an initial stealthy approach, which is generally sufficient to capture prey (32 out of 44 trials). In cases where the initial approach is not sufficient to perform a capture attempt (12 out of 44 trials), *C. townsendii* continues its pursuit by reacting to prey movements in a manner best modeled with a combination of pure pursuit, or following prey directly, and proportional navigation, or moving to an interception point.

AKNOWLEDGEMENTS

We thank Brooke Quinn and Jonas Håkansson for their valuable comments on earlier versions of this manuscript, Mark Thiessen whose photographs of *C. townsendii* were used to produce figures, and Brown University's Center for Computation and Visualization whose computational resources were used to conduct pursuit simulations.

Author contributions. AJC performed the experiments. AB, AJC, HV, and SMS interpreted the results. AB performed the analysis and wrote the manuscript with guidance from AJC, HV, and SMS.

Funding. Experiments and data acquisition was funded by NSF grants (IOS-0951160 and IOS-1257248 to William Conner) and a Theodore Roosevelt grant from the American Museum of Natural History (to AJC). Data

35 processing and analysis and writing of this manuscript was funded by NSF IOS-1931135 (to SMS) and 1931200
36 (to AJC), and a National Science and Technology Council (CONACYT) fellowship (to AB).

37 **DATA AVAILIABILITY**

38 https://doi.org/10.5061/dryad.05qfttf7j

1. Introduction

Predation events are ideal systems to study the interaction of locomotion and ecology because they require a rapid sequence of complex maneuvers and entail life or death consequences [1,2]. The diverse ensembles of modes of predation and prey defenses compete in an evolutionary race for feeding and survival that directly impact fitness [3]. One such mode is predatory pursuit [2]. This is an often demanding task of prolonged duration, in which the environment may dynamically vary given the potential presence of obstacles or resource competitors. A predator's ability to capture its prey during pursuit is, in part, contingent on specializations of its locomotor system, such as the capacity of its sensing apparatus to detect its prey throughout the interaction. Similarly, a key component of a predator's locomotor behavior is its hunting approach or pursuit strategy [4], that is, the rules that describe how a predator should steer to capture moving prey. The collection of these rules is categorized as a type of a behavioral algorithm [5] in which animal form and function interact with the environment to influence ecological outcomes. Behavioral algorithms of this kind have been shown to accurately model predatory pursuit across a range of species, including birds [6], insects [7], bats [8], terrestrial quadrupeds [9], and fish [4]. Although these works often model predator trajectories accurately, they represent a small fraction of the possible realizations of predatory pursuit in nature. Because few species have been studied to date, clear relationships between a species' feeding ecology and specific behavioral algorithms or phylogenetic patterns of algorithmic evolution have yet to be recognized [10].

The study of strategic pursuit behavior in aerial foragers specifically is represented by analyses of only a few species of bats, birds, and insects. The morphological traits that enable powered flight in these groups differ substantially and are well-studied. For instance, bats alone possess wings with numerous flexible joints that allow for substantial shape changes during the wingbeat cycle [11,12], highly compliant skin [13], and relatively heavy wings that facilitate complex aerial maneuvers by controlling inertial forces [14,15]. Another contrasting trait is the mechanism for prey detection, for which birds and insects rely primarily on visual cues [16–20], while bats primarily utilize auditory information [8,21,22]. Although we recognize ways that bats differ fundamentally from birds and insects, we have yet to describe how strategic pursuit behavior differs within and among groups. Therefore, the study of insect predation by bats that employ aerial hawking, flying pursuit of actively flying prey, contributes to understanding the link between an animal's sensorimotor apparatus, feeding ecology, and evolutionary history on the one hand with their steering behavior during foraging on the other.

In this study, we detail the pursuit behavior of the insectivorous Townsend's big-eared bat, *Corynorhinus townsendii.* This distinctive aerial hawking bat hunts stealthily at very low speeds with a characteristic form of echolocation that reduces the prevalence of defensive behaviors by prey and performs complex acrobatic maneuvers, all of which differentiates its flight performance and feeding ecology from bats whose predatory pursuit has been studied previously [8,23–28]. Our work tests the hypothesis that *C. townsendii*'s pursuit behavior differs from other aerial predators according to its distinctive flight abilities and stealth hunting approach. To investigate this, we modeled *C. townsendii*'s pursuit using the combined guidance effects of pure pursuit, which commands a predator to follow prey directly, and proportional navigation, in which the predator moves to an interception point. To integrate the unique steering commands generated by these components in

a meaningful way, we employ a mixed model guidance control algorithm similar to previous studies in this field [6,29].

List of symbols and abbreviations	
FOC	Global frame of coordinates
$\boldsymbol{r}$	Predator-prey distance; line-of-sight (m)
$\boldsymbol{v}$	Velocity (ms^{-1}) $\boldsymbol{v}_p$: predator; $\boldsymbol{v}_t$: prey
$\boldsymbol{a}$	Acceleration (ms^{-2})
$\boldsymbol{a}_{vl}$	Tangential acceleration (ms^{-2})
$\boldsymbol{a}_{en}$	Engagement acceleration/steering (ms^{-2})
$\boldsymbol{a}_{nr}$	Normal acceleration (ms^{-2})
$\boldsymbol{a}_{st}$	Steering acceleration (ms^{-2})
d_c	Osculating circles' center-to-center distance (cm)
a^*_{vl}	Tangential acceleration trend score
FOC′	Frame of coordinates during the repositioning phase
$\boldsymbol{x}',\boldsymbol{y}',\boldsymbol{z}'$	Orthogonal basis of FOC′
$\hat{\boldsymbol{\imath}},\hat{\boldsymbol{\jmath}},\hat{\boldsymbol{k}}$	Unitary vectors of the engagement coordinate system
PP	Pure pursuit
PN	Proportional navigation
K_{PP}	Pure pursuit gain
K_{PN}	Proportional navigation gain
δ	Angle between the line-of-sight $\boldsymbol{r}$ and $\boldsymbol{v}_p$ (°)
$\boldsymbol{\omega}_r$	Rate of rotation of the line-of-sight vector (rad/s^{-1})
τ	Predator sensorimotor delay (s)
RMSE	Root mean squared error
NRMSE	RMSE normalized by $\lvert\boldsymbol{r}\rvert$

2. Methods

Study species

Townsend's big-eared bat, *Corynorhinus townsendii* (fig. 1), an insectivorous member of the Vespertilionidae, ranges from southern Canada and western North America to southern Mexico [30]. Its wingspan averages 28.5cm, body weight averages 10 grams [30–32], and average body length is 5.75cm (from nose to base of tail) [33]. They typically roost in caves and mines and usually hunt no further than 10km from the roost [34,35]. They forage using predominantly slow, maneuverable flight close to vegetation [31]. Their large ears, around one-third of their body length [30], may provide additional lift [36] in addition to their primary auditory function, including in prey detection. Their echolocation intensity is relatively low compared to other bat species, which causes their insect prey to exhibit fewer defenses [37].

Figure 1: *Corynorhinus townsendii.* A) A bat being held by an observer wearing a nitrile glove. B) A bat pursuing a moth moments before a capture attempt. Photographs by Mark Thiessen.

Animal care

All vertebrate animal use was approved by the Wake Forest University Animal Care and Use Committee (IACUC protocol A12-048). Bats were captured using mist nets placed in riparian areas at the American Museum of

Natural History's Southwestern Research Station (SWRS) in Portal, Arizona. After capture, bats were allowed to fly and hunt free-flying insects for 1-2h for two nights so they could adjust to captivity and were held for four additional nights for flight experiments. When not flying, bats were held in a custom cage (30x50cm floor, 30cm high) with access to water and grouped together to provide social interaction. Moths and other insects were also collected within the SWRS using 15W ultraviolet light live traps (Leptraps LLC, Georgetown, KY, USA) with 5 gallon containers.

Experimental design

We recorded the predatory behavior of *Corynorhinus townsendii* while hunting free-flying insects inside an outdoor flight enclosure (6x4m floor, 2.3m high; 1mm cloth wire and 10mm square spacing) at the SWRS in June 2012. Bats ($n = 4$) were released one at a time inside the enclosure and began feeding shortly after entering. Their hunting and flight behavior indicated a high level of comfort within the flight arena. To maximize the number of optimal recordings, no more than 1-5 insects were allowed to fly at a time within the enclosure. As bats fed, additional insects were introduced by manually controlling a partially closed insect container on the floor. Two 60mW UV LEDs (5mm, 395nm) were placed within the observation space, separated by 1.5m, to attract the insects and thereby encourage bats to hunt within the cameras' field of view. Bats were captured after they showed signs of satiation such as ceasing to hunt, frequent landing on the enclosure walls, or ceasing to fly for an extended period. Typically, an individual would forage for 20 to 60 min. At this point, the subject was removed from the enclosure and a different individual was released. This process was repeated for four nights of recording.

Video was captured by three frame-synchronized, IR-sensitive cameras (scA640-120gc Basler, Inc., Ahrensburg, Germany) recording at a resolution of 656x494 and a speed of 90fps. The combined in-focus field-of-view of the cameras resulted in an observation volume measuring approximately 4.5x3x2m(*w* x *l* x *h*). Video was acquired using maxTraq 2.0 software (Innovision Systems Inc., Columbiaville, MI, USA). The enclosure was illuminated by two Raymax 200 Platinum infrared lights (Raytec, Ashington, UK). Bat echolocation calls were recorded using four Avisoft CM16/CMPA ultrasound microphones and an UltraSoundGate 416H recording unit (Avisoft Bioacoustics, Brandenburg, Germany), which was connected to the camera's synchronization signal. All cameras were set to continuously record 90-second flight bouts separated by a 15-second downtime to transfer the on-board memory recordings to a hard drive. A previous study by Corcoran & Conner (2017) [37] originally acquired and utilized the full set of data to study predator counteradaptations to prey evasive maneuvers; readers should refer to this publication for further methodological details.

Data processing

All trial videos were manually inspected and categorized according to the bat's behavior. From the 226 recorded predator-prey interactions, we observed 9 in which the moth successfully avoided capture, 9 in which the bat gleaned the moth from the enclosure's wall, 28 in which bats aborted apparent pursuit before reaching the prey, and 180 where the bat successfully captured the moth. 136 of the latter category were excluded from further analysis because most or all of the pursuit trajectory occurred outside the combined observation volume

of the cameras, or because the calibration procedure for that day yielded poor accuracy. Only the remaining 44 successful capture trials ($n = 3$ bats) were employed in further analysis and were manually digitized in MATLAB R2021b (Natick, MA, USA) using DLTdv8a [38]. The cameras' 2D views were calibrated and transformed into 3D coordinates using a "wand" calibration process [39], for which videos were recorded every night using a 0.75m wand. Bats were represented as a single digitized point located approximately at the intersection of the subjects' coronal and sagittal planes and a transverse plane crossing the shoulder blades. Moths, generally just a few pixels in size, were also digitized as a single point. The three-dimensional positional data was first smoothed using a symmetric moving average filter of 4 samples followed by a Savitzky-Golay filter with a symmetrical window size of 12 samples. Lastly, the data were fit using MATLAB's *smoothing spline* function to procure smooth time derivatives. The degree of this spline fit was determined on a trial-by-trial basis under the condition that the resulting coordinates did not deviate from the originally digitized points by more than 8mm on average for a bat and 3mm for a moth (around 13% and 30% of body length respectively) [30]. Velocity and acceleration vectors were calculated by differentiation of the filtered position data. Additionally, predator acceleration was decomposed into the following components (fig. 2-A): tangential acceleration ($\boldsymbol{a}_{vl}$), which changes velocity magnitude; steering acceleration ($\boldsymbol{a}_{st}$), which directs the change in heading; engagement acceleration ($\boldsymbol{a}_{en}$), or the component of $\boldsymbol{a}_{st}$ which lies in the engagement plane, where the prey is found; and normal acceleration ($\boldsymbol{a}_{nr}$), or the component of $\boldsymbol{a}_{st}$ which is orthogonal to the engagement plane along $\hat{\boldsymbol{k}}$

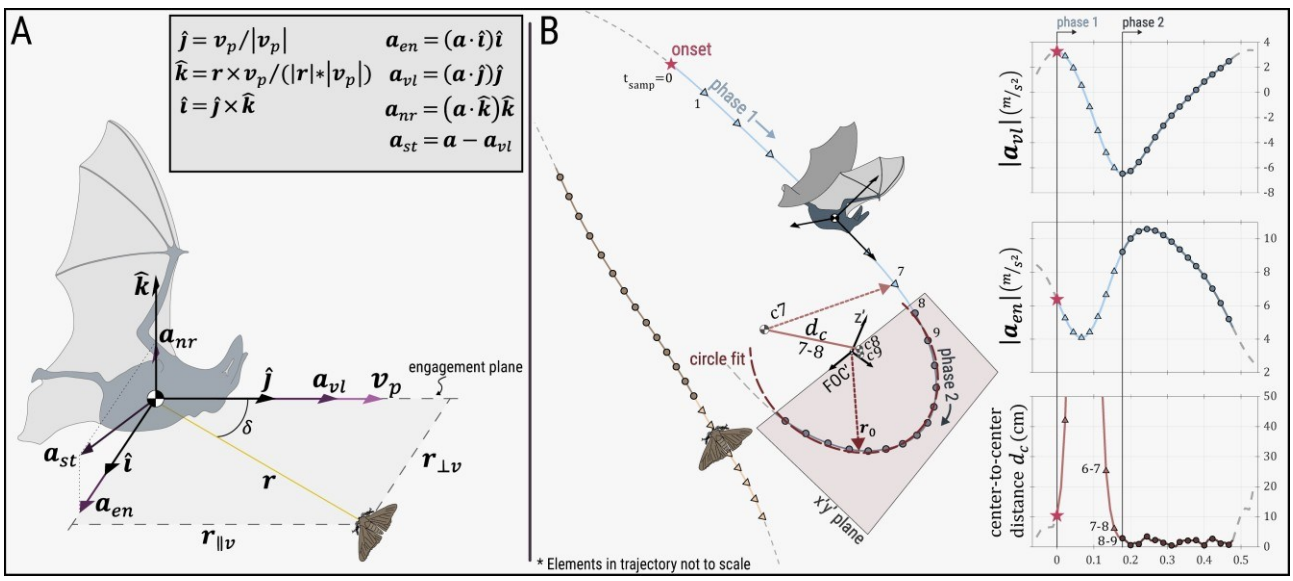

Figure 2: A) Definition of the geometry of the engagement. The bat's body orientation may not align with the coordinate system as displayed. Predator acceleration is decomposed in the following components: tangential acceleration ($\boldsymbol{a}_{vl}$), steering acceleration ($\boldsymbol{a}_{st}$), engagement acceleration ($\boldsymbol{a}_{en}$), and normal acceleration ($\boldsymbol{a}_{nr}$). B) A pursuit trajectory showing the bat moving through Phase 1 (assessment; triangles) and 2 (repositioning; circles). Each marker represents a digitized point; indices of t_{samp} represent frame numbers recorded at 90fps. After onset, or the start of Phase 1, the tangential acceleration magnitude ($|\boldsymbol{a}_{vl}|$) decreases (top), while the engagement steering magnitude ($|\boldsymbol{a}_{en}|$) increases until it reaches a peak value during Phase 2 (middle). The dotted arrow and center symbol *c7* represent the osculating circle defined by points 6, 7, and 8. The segment *7-8* measures the distance between centers *c7* and *c8*. The length of these segments, the osculating circles' center-to-center distance, d_c, declines to define the beginning of Phase 2 (bottom). The coordinate system FOC' and $x'y'$ plane are the result of the singular value decomposition of the trajectory points during Phase 2. The dotted arrow $\boldsymbol{r}_0$ represents the radius of the circle fitted to the observed trajectory points during Phase 2 in FOC'.

Mathematical modeling

To analyze the predators' behavior leading to prey capture, we searched for flight kinematic patterns associated with prey detection. Scalar symbols are represented in regular typeface, vector symbols in bold typeface, and vector magnitude by single vertical bars. We annotated the approximate frame where the predator directs and subsequently maintains orientation of its head towards the prey; we designated this as a proxy for attention and prey detection (S1 Video). Typically, five or fewer frames later we observed a local peak in the magnitude of the bats' tangential acceleration ($|\boldsymbol{a}_{vl}|$; fig. 2-B), which we defined as the onset of pursuit. To distinguish between equal values of $|\boldsymbol{a}_{vl}|$ with different rates of change, we computed the score:

$$a^*_{vl}(t) = |\boldsymbol{a}_{vl}(t)| * \frac{\dot{a}_{vl}(t)}{\|\dot{a}_{vl}(t)\|} \qquad (2.1)$$

where $|\boldsymbol{a}_{vl}|$ is the magnitude of tangential acceleration and $\dot{a}_{vl}$ its time derivative. The term $\dot{a}_{vl}/\|\dot{a}_{vl}\|$ accounts for increasing vs. decreasing trends in acceleration at time t. We confirmed the significance of this change by a statistical comparison of the distribution of a^*_{vl} before and after onset using an 11 sample window ($t \approx 0.12$s). In the few trials where the score as defined above did not yield statistically significant results, generally because bats were already decelerating, we defined the pursuit onset as beginning at the frame in which we observed the bat's gaze to be directed at the prey.

The Assessment phase was followed by a Repositioning phase (see Results for descriptions of pursuit phases), which consisted of a single turn maneuver. By manual inspection, we found that this turn occurred approximately in a single plane. We defined the start of this phase when $d_c < 4.5cm$ (fig. 2-B), or when the bat's center of rotation at time t, an osculating circle, was less than $4.5\mathrm{cm}$ from that at $t+dt$; that is, when the bats were turning about a near-constant center of rotation. To model the kinematics of this motion we established a new frame of coordinates, FOC' (fig. 2-B) by carrying out a singular value decomposition of the observed 2D position values and assigning the $x'y'$ plane as the principal plane of motion. Then, we modeled this turn maneuver as a circle (fig. 2-B):

$$(x' + b_1)^2 + (y' + b_2)^2 = {r_0}^2 \qquad (2.2)$$

where r_0 is the circle's radius, b_1 and b_2 are unknown constants, and x' and y' are the coordinates of the observed trajectory points based on FOC'. We utilized a non-linear regression fit model to find the best estimates for r_0, b_1, and b_2. The resulting root-mean-square error, normalized by the turning radius, (NRMSE) was used to evaluate the model's fit.

We approximated the predator's aggregate change in heading over a pursuit phase by:

$$\psi = \sum_{k=2}^{N} \cos^{-1}(\hat{\boldsymbol{v}}_k \cdot \hat{\boldsymbol{v}}_{k-1}) \qquad (2.3)$$

where $\hat{\boldsymbol{v}}$ is the normalized velocity vector, N is the total number of samples, and ψ is the approximate total change in heading.

When comparing a measure between groups of trials for which we know the mean and standard deviation for each trial, we utilized a generalized mean and standard deviation to account for differences in sample sizes whenever relevant as follows:

$$\bar{X} = \frac{1}{\sum_{k=1}^{N} n_k} \sum_{k=1}^{N} n_k * \bar{x}_k \tag{2.4}$$

$$\mathrm{SD}^2 = \frac{1}{\sum_{k=1}^{N} n_k} \sum_{k=1}^{N} n_k * (\sigma_k^{\,2} + \bar{x}_k^{\,2}) - \bar{X}^2 \tag{2.5}$$

where $\bar{x}$, σ, and n are the measured mean, standard deviation, and number of samples respectively for a trial; N is the total number of trials in the group; and $\bar{X}$, and SD are the generalized mean and standard deviation of the group of trials.

Statistical analysis

We analyzed the distribution of computed measures and report the median ($\tilde{x}$) and interquartile range (IQR) to account for outliers and skew; whenever data were normally distributed, we report the mean and standard deviation. All statistical tests' null hypotheses were rejected at the 5% significant level ($\alpha = 0.05$). When statistical tests were performed in multiple trials but summarized as a group, we report the maximum p-value ($p_{\max}$) for interpretation.

We used a Wilcoxon rank sum test (U) to check for differences in the median values of two non-normally distributed samples. When testing if a sample's median differed from zero, we instead used a one-sample Wilcoxon signed rank test (U_0).

To test the hypothesis that a trajectory predicted by the pursuit model (eq. 2.12) did not differ significantly from that created by the processed data, we employed a two-sample Kolmogorov-Smirnov test (KS) on each Cartesian global coordinate as a generalized proxy for goodness-of-fit [4].

Simulations

We composed a guidance control model that would predict the predator's flight during Phase 3 of pursuit (Chase) based on our initial assumptions and prior work in this field [4,6,29,40,41]. Our mixed model considered the combined effects of pure pursuit and proportional navigation components [42], as well as each strategy independently. If a predator's pursuit was governed solely by pure pursuit, its steering command would be proportional to the angle delta:

$$a_{\mathrm{cmd}|PP} = K_{PP} * \delta \tag{2.6}$$

where K_{PP} is the pure pursuit component's gain and δ is the angle between the predator's heading and the line-of-sight vector (fig. 2-A). Under this rule, $a_{\mathrm{cmd}|PP}$ aims to drive δ to zero; that is, the predator would constantly attempt to follow its target directly (fig. 3). To implement a guidance law based on this rule, expressed in vector notation, we first include an odd-symmetric sine function [42] to increase the command's gain value at

moderate to high angles while, maintaining it at low values of delta given $\sin(\delta) \approx \delta$ for small angles. Note that the use of this function has no geometric meaning. Additionally, we incorporate the predator's velocity ($\boldsymbol{v}_p$) as a dynamic gain to increase the steering command proportionally with speed. Under pure pursuit guidance, $\boldsymbol{a}_{cmd|PP}$ only acts in the engagement plane; i.e., $\boldsymbol{a}_{\mathrm{cmd}|PP} \times \hat{\boldsymbol{\imath}} = 0$.

$$\boldsymbol{a}_{\mathrm{cmd}|PP} = K_{PP}[\boldsymbol{v}_p \times \sin(\delta)\hat{\boldsymbol{k}}] \tag{2.7}$$

$$\delta = \cos^{-1}\left(\frac{\boldsymbol{r}}{|\boldsymbol{r}|} \cdot \hat{\boldsymbol{\jmath}}\right) \tag{2.8}$$

If a predator's pursuit was dictated by a proportional navigation strategy, then its steering command would be proportional to the rate of rotation of the line-of-sight vector [42]:

$$a_{\mathrm{cmd}|PN} = K_{PN} * v_p * \lambda \tag{2.9}$$

where K_{PN} is the proportional navigation component's gain, λ is the rate of rotation of the line-of-sight vector, $\boldsymbol{r}$, and v_p is the predator's speed. Under this rule, and with $K_{PN} = 1$, the predator will steer to match the rate of rotation of the line-of-sight vector, which, for a non-maneuvering prey moving at constant speed, would result in making $\boldsymbol{r}_t$ remain parallel to $\boldsymbol{r}_{t-dt}$ (fig. 3). To implement a guidance law based on this rule we replace λ with its generalized vector form $\boldsymbol{\omega}_r$:

$$\boldsymbol{\omega}_r = \frac{\boldsymbol{r} \times (\boldsymbol{v}_t - \boldsymbol{v}_p)}{|\boldsymbol{r}|^2} \tag{2.10}$$

Finally, for this analysis, we considered the effect of proportional navigation component in the engagement plane only:

$$\boldsymbol{a}_{\mathrm{cmd}|PN} = K_{PN}([\boldsymbol{\omega}_r \times \boldsymbol{v}_p] \cdot \hat{\boldsymbol{\imath}})\hat{\boldsymbol{\imath}} \tag{2.11}$$

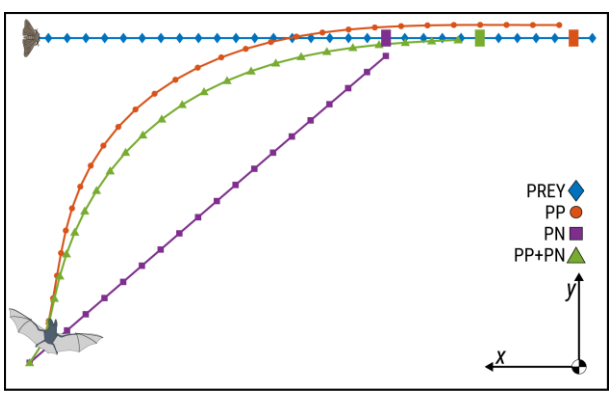

Figure 3: A simulated 2-dimensional trajectory depicting predator's responses to the prey flight path based on pure pursuit, proportional navigation, and mixed model strategies with gains $K_{PP} = 1$ and $K_{PN} = 1$, and predator-prey speed ratio $|\boldsymbol{v}_p|/|\boldsymbol{v}_t| = 1.4$. Rectangles mark the point of capture in each strategy.

We recreated the predators' chase phase by calculating its engagement steering ($\boldsymbol{a}_{en}$; fig. 2-A) based on a mixed-guidance control model with both pure pursuit and proportional navigation components. A time delay τ was incorporated into the prey's observed kinematics to account for the predator's sensorimotor delay as follows (fig. 4):

$$\boldsymbol{a}_{en}(t) = K_{PP}[\boldsymbol{v}_p(t) \times \sin(\delta(t-\tau))\hat{\boldsymbol{k}}] + K_{PN}([\boldsymbol{\omega}_r(t-\tau) \times \boldsymbol{v}_p(t)] \cdot \hat{\boldsymbol{\imath}})\hat{\boldsymbol{\imath}}, \qquad |\boldsymbol{a}_{en}| \leq |\boldsymbol{a}_{\max}| \tag{2.12}$$

To predict the predator's hunting behavior, we generated time-discrete simulations of virtual predators whose engagement steering was ruled by equation 2.12. A simulation consisted of generating a trajectory by providing the prey's observed motion at time $t - \tau$; the predator's observed tangential and normal accelerations at time t; a set of variables $\{K_{PP}, K_{PN}, \tau, |\boldsymbol{a}_{\max}|\}$; and the virtual predator's position, heading, and speed from a previous iteration. To start the solver's first iteration, we provided the predator's observed kinematics as initial conditions (fig. 4).

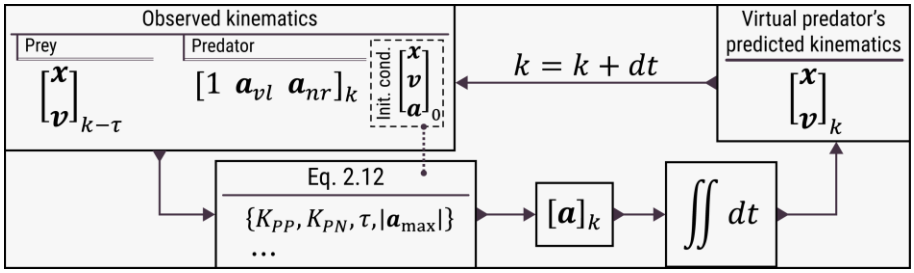

Figure 4: Schematic of simulation computation. For a given set of variables (brackets) and initial conditions (dotted line and dotted box), the observed kinematics are used to generate steering commands for the virtual predator. Using this acceleration, the solver computes the virtual predator's position and velocity.

To find sets of values that would best recreate the bat's flight behavior, we performed an exhaustive parameter search simulating all permutations resulting from a pure pursuit with gain ranging from 0 to 10 (K_{PP} : $\{n/4 \mid n \in [0, \dots, 40]\}$), a proportional navigation with gain ranging from 0 to 5 (K_{PN} : $\{n/4 \mid n \in [0, \dots, 20]\}$), with values of sensorimotor delay ranging from 0.1 to 0.2s (τ : $\{n/100 \mid n \in [10, \dots, 20]\}$), and with maximum steering acceleration between 6 to 16ms^{-2} ($|\boldsymbol{a}_{\max}|$: $\{n \mid n \in [6, \dots, 16]\}$). A gain of zero for either of the models' components was included to test the hypothesis that one strategy alone could explain the predator's steering. The selected range for K_{PP}, K_{PN}, and τ were informed by previous work in this field [6,19,29,40,41,43,44], and the acceleration limits were set by our manual inspection of the predators' observed acceleration range in this study. We varied the starting point of the simulation from $t = 0$ to $t = 0.2t_{\text{end}}$ to account for transient effects in the predator's dynamics between Phases 2 (Repositioning) and 3 (Chase).

Simulations were terminated if the predator's predicted position deviated from the observed trajectory by more than 5cm. We selected a maximum of 100 best-fitting solutions per trial, defined as those that predicted the greatest fraction of the bat-moth interaction and that had an RMSE of less than 1.5cm. For trials with fewer solutions, we relaxed the RMSE constraint to 3.5cm. The best-fitting solutions from all trials were grouped to form a globally-fitted set that represents our best estimate of the pursuit behavior for this species (fig. 6-A). An evaluation of the noise sensitivity of this modeling approach can be found in the supplemental material (S8 Appendix).

3. Results

Onset of pursuit

Following bats' initial prey detection, we observed a significant change in the predator's acceleration profile: the distribution of the tangential acceleration scores (a^*_{vl}) after onset (detection) declined in most trials (U: $p_{\max} < 0.03$; $n = 40$). Specifically, bats reduced tangential acceleration which resulted in a value of a^*_{vl}that was 22% lower after compared to before onset (IQR: $14.7{\sim}31.5$; $n = 37$); three outlier trials in which bats decelerated had a higher drop in the a^*_{vl} score ($119{\sim}320\%$). The deceleration response to the prey's presence at onset occurred

at a range of distances ($|\tilde{\boldsymbol{r}}| = 0.71\text{m},\ \text{IQR: } 0.50\sim0.90$) and, for this species and compared to later phases of pursuit, at relatively high speeds ($|\tilde{\boldsymbol{v}}| = 2.74\ \text{m/s}, \text{IQR: } 2.14\sim3.35$) [45].

Phase 1: Assessment

Throughout the relatively short Assessment phase ($\tilde{t} = 0.23\text{s}, \text{IQR: } 0.18\sim0.27$), bats maintained generally straight forward flight; median change in heading ($\tilde{\psi}$) in the first half of this phase was $6.7°$ ($\text{IQR: } 4.6\sim8.7$) over a total distance of 0.28m ($\text{IQR: } 0.10\sim0.44$). The decline in tangential acceleration magnitude ($|\boldsymbol{a}_{vl}|$), which signaled the onset of pursuit, continued to decrease from its peak (e.g., fig. 2-B), and soon after pursuit onset, we observed an increase in the steering acceleration magnitude ($|\boldsymbol{a}_{st}|$). At the end of Phase 1, $|\boldsymbol{a}_{st}|$ had increased 255% on average relative to its value at pursuit onset ($\text{IQR: } 234\sim279; n = 42$), except in two outlier trials in which the effect was greater ($364\sim409\%$). Increased $|\boldsymbol{a}_{st}|$ arose from an increase of the engagement steering, $|\boldsymbol{a}_{en}|$, the steering component aimed directly at the prey (fig. 2-A). The proportion of steering in the engagement plane ($|\boldsymbol{a}_{en}|^2/|\boldsymbol{a}_{st}|^2$) at the end of this phase averaged 94.3% over all trials ($\text{IQR: } 84.2\sim98.3$), which is significantly greater than the mean at pursuit onset of 80.7% ($\text{IQR: } 48.1\sim95.5;\ U: p < 0.005$). Although the predator-prey distance at the end of this phase varied ($|\tilde{\boldsymbol{r}}| = 0.39\text{m}, \text{IQR: } 0.24\sim0.56$), in most trials the bat-moth vector ($\boldsymbol{r}$) was oriented nearly perpendicular to the bats' velocity vector ($\delta = 82.8°, \text{IQR: } 72.1\sim97.0; n = 39$); that is, $\boldsymbol{r}_{\perp v}$ was the dominant component of $\boldsymbol{r}$ (fig. 2-A).

Phase 2: Repositioning

After Phase 1, bats entered a second, Repositioning phase, characterized by a single turn maneuver of short duration ($\tilde{t} = 0.15\text{s}, \text{IQR: } 0.10\sim0.19$). The distribution of the osculating circles' center-to-center distances (d_c; fig. 5-A) during this phase differed significantly from both other phases ($U: p_{\max} \ll 0.01$). Modeling the near-planar conformation of the bat's maneuver as a circle yielded a median normalized root-mean error (NRMSE) of 8% ($\text{IQR: } 2\sim22; n = 36$). In some trials ($n = 8$), this maneuver had a prominent out-of-plane component (z'); that is, the trajectory resembled a helix rather than a circle, and therefore yielded high fit errors. These maneuvers occurred at a range of linear speeds ($\bar{V} = 1.56\ \text{m/s}, \text{SD} = 0.61$), angular speeds ($\bar{W} = 9.15\ \text{rad/s}, \text{SD} = 4.89$), total heading angle changes ($\tilde{\psi} = 80°, \sigma = 32$), and turning radii ($\tilde{r_0} = 0.18\text{m}, \text{IQR: } 0.10\sim0.24$). The bat's steering, however, continued to be dominated by the component in the engagement plane ($|\boldsymbol{a}_{en}|$). The engagement-to-total steering proportion ($|\boldsymbol{a}_{en}|^2/|\boldsymbol{a}_{st}|^2$) during the first 70% of the maneuver produced a generalized mean of 90.3% ($\text{SD} = 2.8$), which declined to 83.8% ($\text{SD} = 5.8$) for the final 30% of the turn. Additionally, the angle between the bat's velocity vector and the line-of-sight to the prey declined considerably to an average value of $33.5°$ ($\text{IQR: } 24.6\sim47.4$), resulting in the pursuing bat positioned "behind" (posterior to) the prey (fig. 5-B); the spread of headings for the prey differed significantly with an average of $43.0°$ ($\text{IQR: } 26.5\sim66.1; U: p < 0.034$). At the end of this phase, predator-to-prey distances averaged 0.39m ($\text{IQR: } 0.24\sim0.53$), which was not significantly different than the average distance at the start of this phase ($U_0: p > 0.16$).

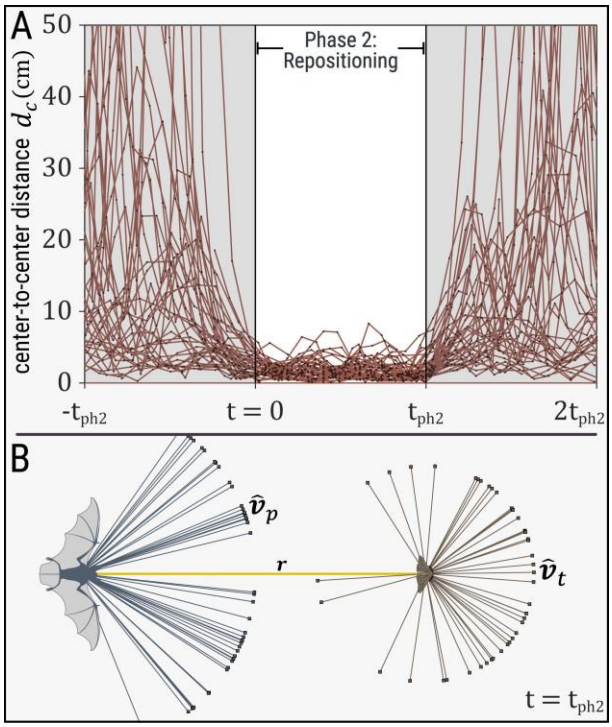

Figure 5: A) The osculating circles' center-to-center distance, d_c (fig. 2-B), for all significant trials ($n = 36$), or those without a prominent z' component. To superimpose all trials, the horizontal time axis has been normalized by t_{ph2}, or the duration of Phase 2. The plot shows how, during Phase 2, bats move in a circular trajectory about a near constant center of rotation. B) The distribution of predator and prey headings at the end of Phase 2. Line and tip plots represent a predator and prey unitary velocity vector, $\hat{\boldsymbol{v}}_p$ and $\hat{\boldsymbol{v}}_t$ respectively. All trials for each (predator and prey) are superimposed to show the spread of headings with respect to the line-of-sight vector ($\boldsymbol{r}$) at $t = t_{\mathrm{ph2}}$. The schematic illustrates how, after the Phase 2 turn maneuver, bats' heading vectors point towards the prey, but the prey's heading generally point away from the bat's.

Chase vs non-chase

We observed two distinct types or classes of flight behavior following the Repositioning phase that we designate as chase and non-chase trials. We categorized a trial as non-chase ($n = 32$) if the time-to-capture after Phase 2 was less than $0.45\mathrm{s}$, a threshold manually selected based on the time-to-capture distribution of all trials (S5 Figure). This yielded an average time-to-capture for non-chase trials of $0.22\mathrm{s}$ ($\mathrm{IQR}: 0.13{\sim}0.32$) and $0.6\mathrm{s}$ ($\mathrm{IQR}: 0.50{\sim}0.77$) for chase trials ($n = 12$). At the start of this phase, we found no significant difference in predator-prey distance ($|\tilde{\boldsymbol{r}}| = 0.39\mathrm{m}, \mathrm{IQR}: 0.24{\sim}0.53;\ U{:}\,p > 0.12$), predator's speed ($U{:}\,p > 0.42$), or predator's acceleration ($U{:}\,p > 0.43$) between groups. Using the prey's acceleration during Phase 2 as a proxy for maneuvering, however, groups differed significantly ($U{:}\,p < 0.011$). That is, when moths accelerated more during the bat's repositioning, the remainder of the interaction became a chase. In the non-chase group, we found no significant difference between the prey's acceleration profile during Phase 2 and the remainder of the pursuit ($U{:}\,p > 0.25$) nor in the speeds at which the bats moved ($U{:}\,p > 0.19$). After the Repositioning phase, non-chasing bats quickly began to perform a capture maneuver (fig. 7-C) but chasing bats did not.

Phase 3: Chase

Interactions that continued to a chase ($n = 12$) included a diverse range of flight kinematics for both predator and prey and thus resulted in a wide variety of trajectory topologies (S6 Appendix). Simulations to model the observed trajectories produced a limited set of best-fitting solutions (fig. 6-A) that predicted most of the interaction ($92.7\%, \mathrm{IQR}: 90.4{\sim}95.4$) and closely approximated the bats' flight behavior with a generalized average RMSE of $1.24\mathrm{cm}$ ($\mathrm{SD} = 0.59$), 1.30% ($\mathrm{SD} = 0.87$) of the instantaneous distance to the prey. No modeled solution differed significantly from the original trajectory according to Kolmogorov-Smirnov tests, except for seven alternative solutions for one specific trial.

There was no single optimal set of input values for equation 2.12 that minimized error globally (across all trials). Instead, the pool of best-fitting solutions resulted in a global distribution of K_{PP} and K_{PN} values (fig. 6-A). Successful solutions were produced by a narrow range of K_{PN} values (IQR: $0.5{\sim}1.25$), and a distribution of K_{PP} values that was sparse and without a clear mode (IQR: $1.25{\sim}4.75$). We found no linear correlation between the distribution trends of K_{PP} and K_{PN} ($p \ll 0.001$). The distribution of K_{PP} values had a significant, negative correlation with prey speed in all trials ($R = -0.66,\ p < 0.02$). In some trials (7 out of 12) the distribution of K_{PP} had a significant, positive correlation with prey acceleration ($R = 0.80,\ p < 0.03$), while in the remaining (5 out of 12) there was no correlation ($p > 0.16$). These five trials had a significantly higher K_{PN} gain ($\tilde{K}_{PN} = 0.92 \text{ vs. } 0.5, U{:}\, p < 0.01$) and occurred at significantly lower prey accelerations ($\tilde{a} = 3.7 \text{ vs. } 6.4\text{ms}^{-2}, U{:}\, p < 0.03$).

The distribution of sensorimotor delay values belonging to the pool of best fitting solutions had an average of $\tilde{\tau} = 0.13\text{s}$ (IQR: $0.11{\sim}0.15$) with no clear mode. Moreover, we found no correlation between sensorimotor delay and K_{PP} or K_{PN} (fig. 6-B). Varying maximum steering acceleration magnitude had no influence on simulations results.

Testing pure pursuit and proportional navigation strategies separately resulted in larger trajectory prediction errors compared to the mixed model (fig. 4-C). Additionally, neither model was able to find solutions for all trials ($N_{PP} = 9, N_{PN} = 11$) and when successful, a single model typically achieved fewer than 40 solutions. The values of K_{PP} and K_{PN} for the single strategy simulations differed significantly from those in the mixed model (fig. 6-D).

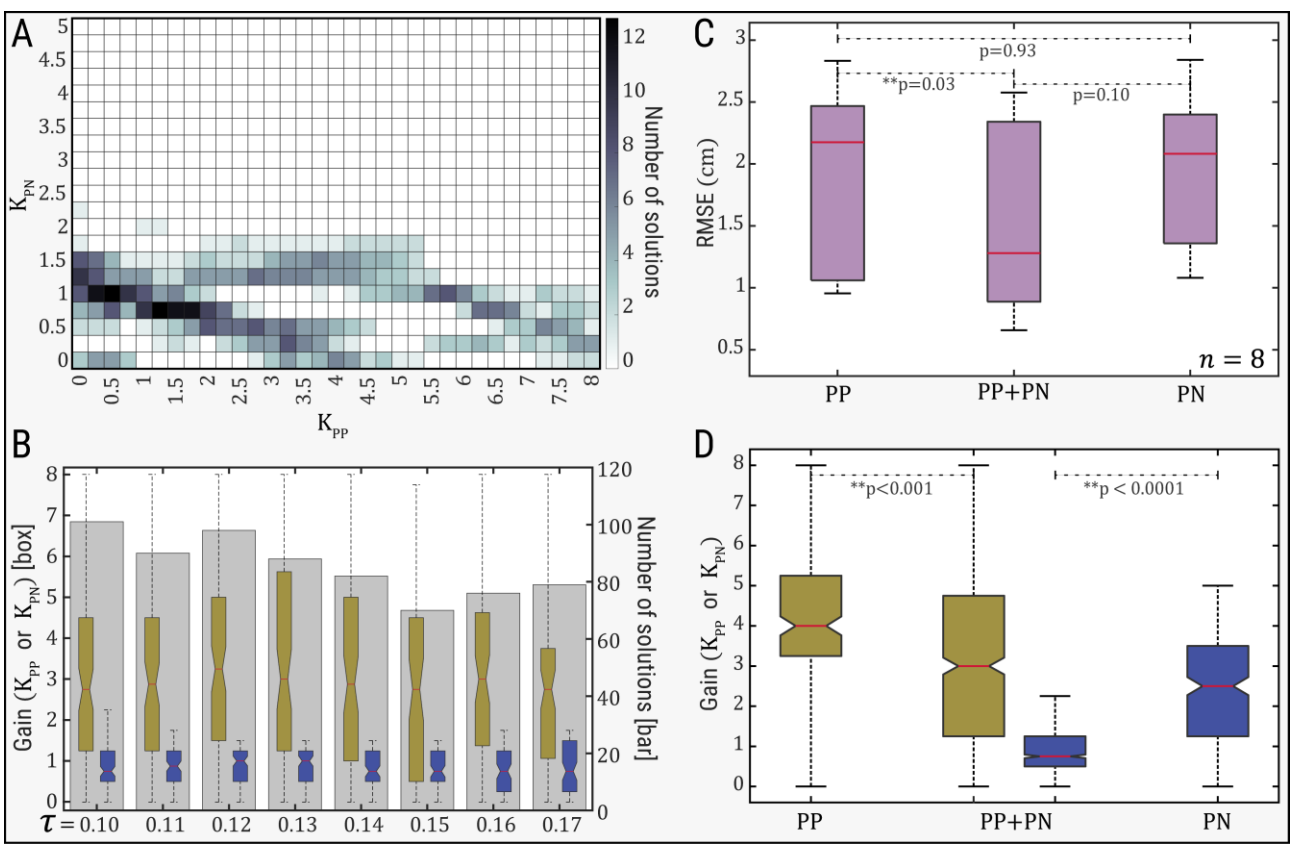

Figure 6: A) Gains of the global (all trials combined) best-fitting mixed model solutions. For each grid cell, the number of solutions is equal to the summation of trials that accurately modeled the predator pursuit with a given K_{PP} and K_{PN} pair; trials varied in their 3D

trajectories, so they differed in the degree to which they are well fit by alternative gains. Each trial is counted, at most, once per grid cell (intensity axis; right). The grid resolution and limits represent the parameter space employed in the simulations. B) The value space sorted by sensorimotor delay magnitude; each box plot pair depicts K_{PP} (yellow) and K_{PN} (blue) distribution (left axis) for a specific sensorimotor delay, τ (horizontal axis). The bar's height (right axis) represents the number of solutions from the best-fitting solutions pool. C) Average RMSE from simulations using pure pursuit (PP), proportional navigation (PN), and the mixed model (PP+PN). Only trials in which all models could be applied are included in results presented (8 out of 12). D) Gain value distribution that produced best-fitting pure pursuit, proportional navigation, and mixed-model solutions. Box plots present interquartile range, whiskers mark minima/maxima, notches represent 95% confidence interval for the median.

4. Discussion

Our in-depth analysis and simulation of *Corynorhinus townsendii's* flight trajectories in successful capture events rejects the hypothesis the strategic predatory pursuit behavior of a highly maneuverable, stealthy, slow-flying bat can be accurately predicted by a single guidance control algorithm [5]. We observed multiple, distinct phases in each capture flight, and this multi-stage strategy differs from classic guidance-controlled pursuit. These phases, Assessment (Phase 1), Repositioning (Phase 2), and finally Chase (Phase 3), are all critical for *C. townsendii*'s hunting success.

Approach: Assessment and Repositioning

During Assessment (Phase 1), bats identify potential prey and begin directed flight, reduce their tangential acceleration, and move with near-linear trajectories. During Repositioning (Phase 2), bats perform a simple, near-planar, near-constant radius turning maneuver initially directed towards the prey, regardless of the details of the prey's motion during this phase.

The approach of *C. townsendii* to moth prey, therefore, demonstrates the following characteristics: simple maneuvers, consistent behavior among individuals and trials, and lack of adherence to a single guidance model (e.g., eq. 2.12). We conclude that, after initial detection, these bats approach prey with movements akin to those of a stereotyped, feed-forward control scheme. Although the mechanistic basis of this feed-forward behavior is unknown, our results show that the execution of Phase 1 and 2 consistently allows predators to reach an advantageous, near-tail chase configuration before continuing with their pursuit (fig. 5-B). This configuration is only beneficial given the short predator-prey distance and low value of δ at the end of Phase 2, and *C. townsendii's* distinct capacity to perform complex maneuvers at low flying speeds thereby allowing this species to respond to prey maneuvers and maintain pursuit [26,46–48].

The specialized hearing and echolocation behavior of *C. townsendii* enables them to detect their prey at $0.8\mathrm{m}$ within and $1.5\mathrm{m}$ outside a flight enclosure [37]. This is consistent with our observations of the onset of pursuit, which estimates detection at an average of $0.71\mathrm{m}$ (IQR: $0.50{\sim}0.90$). In a previous study [37], the bat's quiet echolocation rarely elicited prey avoidance maneuvers. When avoidance behavior was triggered, it was at an average distance of $0.29\mathrm{m}$ ($\mathrm{sd} = 0.17$), approximately the species' wingspan ($28.7\mathrm{cm}$) [31]. Thus, prey potentially detect the pursuing bat just after the Repositioning phase. This suggests that *C. townsendii*'s high prey capture success rate is due, at least in part, to the combination of a stealthy approach and the ability to reach a strategic

location for pursuit before their echolocation calls can be detected by the prey, thereby "revealing" their position.

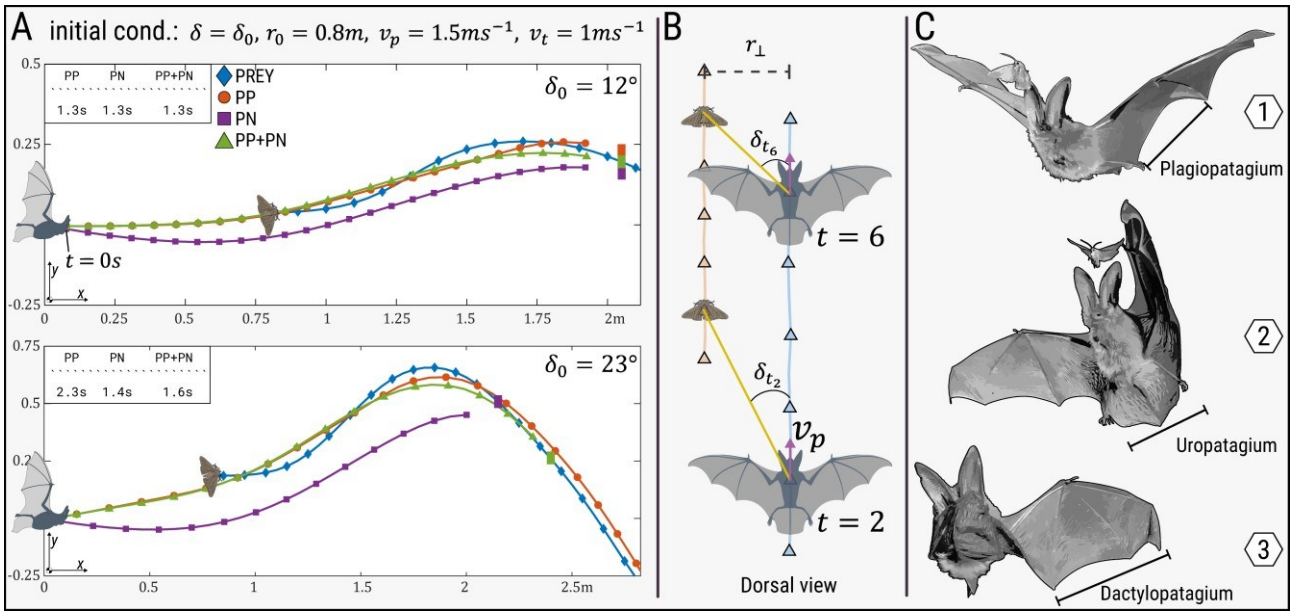

Figure 7: A) Two simulated 2-dimensional trajectories depicting the bat's pursuit response to prey movements using pure pursuit (PP), proportional navigation (PN), and a mixed model (PP+PN) with gains of $K_{PP} = 1.5$ and $K_{PN} = 1$. Prey trajectory in both panels was manually constructed. Colored rectangles mark the capture point for each strategy given an 8cm capture distance between bat and moth centroids. The legend in each plot indicates the capture time in seconds. Top: simulation with a low degree of prey maneuvering and a low starting angle δ_0. Bottom: simulation with high degree of prey maneuvering and starting δ_0. B) Schematic of end of Phase 3. Wings enable long, relatively constant reach, $\boldsymbol{r}_\perp$, just before capture. C) Final approach of stereotypical capture maneuver by *Corynorhinus townsendii*: (1) bat approaches prey; (2) body position reconfigured to catch prey with the distal wing; prey is redirected to the uropatagium (tail membrane) to (3) feed.

Chase

In a minority of cases (12 out of 44), prey capture occurred after a relatively lengthy active chase (Phase 3). Our analysis suggests that the development of this phase was triggered by prey acceleration during the bat's repositioning ($U: p < 0.01$). These prey maneuvers may be a defensive mechanism initiated after predator detection [26,37,46,49], or, alternatively, fortuitous flight movements by the moths. Regardless of the proximate cause of prey acceleration, we accurately predicted flight trajectories of *C. townsendii* with a mixed-model guidance control algorithm (eq. 2.12) with only a small deviation from the observed data ($\text{NRMSE} = 1.30\%, \text{SD} = 0.87$).

The distribution of K_{PP} for the best-fitting solutions (fig. 6-A,D) was broad ($\tilde{K}_{PP} = 3, \text{IQR: } 1.25{\sim}4.75$), consistent with a strong attempt to reduce the value of δ in response to prey maneuvers. High gain values, K_{PP}, translate to a significant requirement for active steering [42], which increases with increasing speed (eq. 2.7). In comparison, a study of Harris' Hawks with an equivalent model found a lower best-fit value of 1 ($\text{IQR: } 0.2{\sim}1.45$) [6]. A pursuer will see little benefit from steering at high values of K_{PP} if their target is distant because flights will become more energetically demanding and require a longer time-to-capture compared to using a PN strategy (fig. 7-A). Nevertheless, at short distances, low initial values of delta, and low flight speeds, the wide range of K_{PP} values

we observe in successful capture flights in this species reflects a substantial capacity to respond to prey maneuvers flexibly and maintain a near-tail-chase pursuit.

The best fitting values for K_{PN} were close to 1 ($\tilde{K}_{PN} = 0.75, \mathrm{IQR}: 0.5{\sim}1.25$), which will make proportional navigation behave similarly to pure pursuit for non-maneuvering targets during tail-chasing, but will result in divergent trajectories for maneuvering prey (fig. 7-A). Predators that forage in the open can realize the intercepting trajectories predicted by higher gain values, such as $K_{PN} \approx 2.6$ in peregrines [40] and $K_{PN} \approx 3$ in robber files [43]. In contrast, interception trajectories of high K_{PN} values may not be viable in denser, more cluttered habitats, where predators forage close to vegetation. In these cases predators may benefit from trajectories that more closely resemble those of their prey; that is, with lower values of K_{PN} [6].

A PN strategy alone, even at $K_{PN} = 1$, can produce trajectories that deviate from the prey's location thereby increasing the probability of encountering obstacles in cluttered environments (fig. 7-A). Conversely, when a predator adopts a PP strategy, the trajectory closely follows the prey but results in a longer time-to-capture and thereby a greater chance for the prey to escape [46,47,50]. Although it requires a greater steering effort than a PN strategy alone, a mixed model delivers a balance between time-to-capture and close fitting trajectories executed by the prey, which may be especially valuable in some microhabitats.

Our results demonstrate that a proportional navigation component is necessary to model *C. townsendii's* pursuit (fig. 6-C). This is, in part, due to how PN turn commands differ from those of PP (S7 Appendix) but may also effectively simulate the bats' capture maneuvers (fig. 7-B,C). *C. townsendii*, like many aerial hawking bat species, generally capture prey with their wings [51]. Multiple parts of the wings can be used for this function, including even the most distal regions of the dactylopatagium (fig. 7-C). Following prey contact with the plagio- or dactylopatagium (arm- or handwing), *C. townsendii* move their prey to the uropatagium, the tail membrane, from which prey is moved to the mouth [51]. As a result, the distance between the body marker in our analyses and the anatomical site of prey capture in this species may be as much as the length of a wing, approximately $10\mathrm{cm}$ [30], which is close to the mean distance between the moth and the pursuing bat at the beginning of Phase 3 ($|\tilde{r}| = 0.39\mathrm{m}, \mathrm{IQR}: 0.24{\sim}0.53$). In some cases (see fig. 7-B), steering in response to the rate of rotation of the line-of-sight may reflect the bat's tendency to approach its prey in a manner compatible with its capture maneuver.

Interpretation of a mixed model

Most studies of aerial predatory pursuit utilize templates [52] of guidance algorithms adapted from the engineering literature whereby a pursuer's steering command is derived from information about itself and its target's motion. For example, pure pursuit produces a steering command which strictly enables a pursuer to move directly towards its target, regardless of the target's motion [42]. A scaling factor or system gain, K_{PP} (eq. 2.7), is incorporated to provide the best fit of the algorithm to a predator's trajectory. This approach models some organisms' pursuit behavior remarkably well [53,54]. Although the control strategy and scaling factor may provide an accurate representation of an organism's locomotor performance during steering in response to prey movements, neither reproduce the organism's pursuit behavior in its entirety. This limits the extent to which they can be interpreted in a biologically meaningful manner, which is in part due to our lack of detailed

knowledge of the cognitive and sensorimotor mechanism underling the locomotor behavior of predatory pursuit.

Modeling the steering of more intricate pursuit behavior or cases that differ significantly from existing guidance algorithms can be complex. Although we can formulate guidance algorithms that uniquely fit a predator's pursuit behavior, adding detail to increase fit may risk losing generality and a biologically meaningful interpretation of models. Alternatively, we may represent complex behaviors by a decomposition using mixed models integrated by multiple, well-defined components. A simplistic example would be to represent bipedal locomotion by a mixed model with two distinct components or ways of moving: walking and jumping. In this view, running, a uniquely distinct gait, could be approximated in the walking vs. jumping space with a high value of walking, and a low and periodical value of jumping. These two components could be thought of as "orthogonal" in the sense that no amount of walking would equate to jumping and vice versa, except when both have value of zero; that is, while standing still. Similarly, a mixed model of predatory pursuit should not be interpreted as a pursuer implementing both strategies simultaneously. Instead, its steering may be well-approximated as a composite of two independent strategies, each of which produces unique responses to a set of inputs, can be interpreted biologically, and shares little overlap with the other in functionality. Such methodology has great potential to model a predator's pursuit behavior because it is robust against as yet unknown systems, allows meaningful conclusions regarding an organism's sensorimotor function during predation, and provides a biologically meaningful framework to compare species.

Matching pursuit guidance to sensory ecology and flight dynamics

Corynorhinus townsendii's strategic pursuit behavior is well-aligned with current understanding of their feeding ecology and the capabilities of their flight apparatus. Their acute hearing, potential detection of prey noises as a stimulus to engage in predatory behavior, and quiet echolocation near prey [37,55] aid their initially stealthy approach. We suggest that this portion of *C. townsendii's* hunting behavior serves to identify the nature of possible prey and provide input to the decision to engage before potentially revealing their presence by their echolocation calls or physical proximity. If pursuit continues, near tail-chase behavior is best modeled by a guidance algorithm that accommodates predator-prey interactions in dense arboreal environments. *C. townsendii* have the highest capture success rate reported for any insectivorous, aerial hawking bat species [37], and the combination of pursuit strategy, sensory capabilities, and flight dynamics could work synergistically to produce this level of performance.

Our conclusion that no single strategy effectively describes the predatory pursuit behavior during aerial hawking in *C. townsendii* differs from previous studies based on other bat species [8,23,25,27,28]. We expect that the group of bat species that employ this feeding mode will possess an ensemble of sensorimotor traits, feeding ecologies, and evolutionary histories that are tightly interwoven with their pursuit behavior, and hence, with the results of this modeling approach. Given the small number of species studied to date, however, it may still be difficult to estimate how disparate pursuit behavior is within this group. In this context, *C. townsendii* provides an important case study [56] because its flight performance may be representative of the highest levels of maneuverability and low flying speeds among aerial hawking bats.

The study of strategic predatory pursuit across taxa, and especially in aerial foragers, has shown that hunting behavior can be well predicted using guidance algorithms [4–8,19,29,54,57]. To date, however, this analysis approach remains limited to inferences of the predator's behavior based on a few variables, such as K_{PP} and K_{PN} as demonstrated here. Development of pursuit models of higher complexity continues actively, and new models incorporate, for example, kinematics and body dynamics of the predator [19] and computational numerical approaches [58–60]. These efforts will expand our understanding of natural behavior in predator-prey interactions to controlled biomechanical experiments in the laboratory [61,62], which include studies of aerodynamic force generation using particle image velocimetry, flapping flight mechanics with high-speed videography in wind tunnels, and detailed characterization of an animal's sensing apparatus.

5. References

1. Irschick DJ, Losos JB. A comparative analysis of the ecological significance of maximal locomotor performance in caribbean anolis lizards. Evolution. 1998;52: 219–226. doi:10.1111/j.1558-5646.1998.tb05155.x

2. Moore TY, Biewener AA. Outrun or outmaneuver: predator-prey interactions as a model system for integrating biomechanical studies in a broader ecological and evolutionary context. Integrative and Comparative Biology. 2015. pp. 1188–1197. doi:10.1093/icb/icv074

3. Dawkins R, Krebs JR. Arms races between and within species. Proc R Soc B. 1979;205: 489–511. doi:10.1098/rspb.1979.0081

4. McHenry MJ, Johansen JL, Soto AP, Free BA, Paley DA, Liao JC. The pursuit strategy of predatory bluefish (*Pomatomus saltatrix*). Proc R Soc B. 2019;286: 20182934. doi:10.1098/rspb.2018.2934

5. Hein AM, Altshuler DL, Cade DE, Liao JC, Martin BT, Taylor GK. An algorithmic approach to natural behavior. Curr Biol. 2020;30: R663–R675. doi:10.1016/j.cub.2020.04.018

6. Brighton CH, Taylor GK. Hawks steer attacks using a guidance system tuned for close pursuit of erratically manoeuvring targets. Nat Commun. 2019;10: 2462. doi:10.1038/s41467-019-10454-z

7. Noest RM, Jane Wang Z. A tiger beetle's pursuit of prey depends on distance. Phys Biol. 2017;14: 026004. doi:10.1088/1478-3975/aa62b9

8. Ghose K, Horiuchi TK, Krishnaprasad PS, Moss CF. Echolocating bats use a nearly time-optimal strategy to intercept prey. PLoS Biol. 2006;4: 865–873. doi:10.1371/journal.pbio.0040108

9. Wilson RP, Griffiths IW, Mills MG, Carbone C, Wilson JW, Scantlebury DM. Mass enhances speed but diminishes turn capacity in terrestrial pursuit predators. Couzin ID, editor. eLife. 2015;4: e06487. doi:10.7554/eLife.06487

10. Taylor G, Thomas A. Evolutionary biomechanics: selection, phylogeny, and constraint. OUP Oxford; 2014.

11. Riskin DK, Willis DJ, Iriarte-Díaz J, Hedrick TL, Kostandov M, Chen J, et al. Quantifying the complexity of bat wing kinematics. J Theor Biol. 2008;254: 604–615. doi:10.1016/j.jtbi.2008.06.011

12. Aldridge HD. Kinematics and aerodynamics of the greater horseshoe bat, *Rhinolophus ferrumequinum*, in horizontal flight at various flight speeds. J Exp Biol. 1986;126: 479–497. doi:10.1242/jeb.126.1.479

13. Cheney JA, Konow N, Bearnot A, Swartz SM. A wrinkle in flight: the role of elastin fibres in the mechanical behaviour of bat wing membranes. J R Soc Interface. 2015;12: 20141286. doi:10.1098/rsif.2014.1286

14. Boerma DB, Breuer KS, Treskatis TL, Swartz SM. Wings as inertial appendages: how bats recover from aerial stumbles. J Exp Biol. 2019;222: jeb204255. doi:10.1242/jeb.204255

15. Bergou AJ, Swartz SM, Vejdani H, Riskin DK, Reimnitz L, Taubin G, et al. Falling with style: bats perform complex aerial rotations by adjusting wing inertia. PLoS Biol. 2015;13: 1002297. doi:10.1371/journal.pbio.1002297

16. Kane SA, Zamani M. Falcons pursue prey using visual motion cues: new perspectives from animal-borne cameras. J Exp Biol. 2014;217: 225–34. doi:10.1242/jeb.092403

519 17. Gibson JJ. Visually controlled locomotion and visual orientation in animals. Br J Psychol. 1958;49.
520 doi:10.1111/j.2044-8295.1958.tb00656.x

521 18. Srinivasan MV, Xiang W. Visual tracking of moving targets by freely flying honeybees. Vis Neurosci. 1990;4:
522 379–386. doi:10.1017/S0952523800004582

523 19. Mischiati M, Lin HT, Herold P, Imler E, Olberg R, Leonardo A. Internal models direct dragonfly interception
524 steering. Nature. 2015;517: 333–338. doi:10.1038/nature14045

525 20. Collett TS, Land MF. Visual control of flight behaviour in the hoverfly *Syritta pipiens* L. J Comp Physiol.
526 1975;99: 1–66. doi:10.1007/BF01464710

527 21. Kalko EKVV, Schnitzler H-UU, Kalko EKVV. Echolocation by insect-eating bats. BioScience. 2001;51: 557–
528 569. doi:10.1641/0006-3568(2001)051[0557:ebieb]2.0.co;2

529 22. Conner WE, Corcoran AJ. Sound strategies: the 65-million-year-old battle between bats and insects. Annu
530 Rev Entomol. 2012;57: 21–39. doi:10.1146/annurev-ento-121510-133537

531 23. Ghose K, Triblehorn JD, Bohn K, Yager DD, Moss CF. Behavioral responses of big brown bats to dives by
532 praying mantises. J Exp Biol. 2009;212: 693–703. doi:10.1242/jeb.019380

533 24. Fujioka E, Aihara I, Sumiya M, Aihara K, Hiryu S. Echolocating bats use future-target information for
534 optimal foraging. Proc Natl Acad Sci U S A. 2016;113: 4848–52. doi:10.1073/pnas.1515091113

535 25. Chiu C, Reddy PV, Xian W, Krishnaprasad PS, Moss CF. Effects of competitive prey capture on flight
536 behavior and sonar beam pattern in paired big brown bats, *Eptesicus fuscus*. J Exp Biol. 2010;213: 3348–56.
537 doi:10.1242/jeb.044818

538 26. Corcoran AJ, Conner WE. How moths escape bats: predicting outcomes of predator-prey interactions. J Exp
539 Biol. 2016;219: 2704–2715. doi:10.1242/jeb.137638

540 27. Vanderelst D, Peremans H. Modeling bat prey capture in echolocating bats: the feasibility of reactive
541 pursuit. J Theor Biol. 2018;456: 305–314. doi:10.1016/j.jtbi.2018.07.027

542 28. Kong Z, Özcimder K, Fuller NW, Theriault D, Betke M, Baillieul J. Perception and steering control in paired
543 bat flight. IFAC Proc Vol. 2014;47: 5276–5282. doi:10.3182/20140824-6-ZA-1003.01670

544 29. Brighton CH, Chapman KE, Fox NC, Taylor GK. Attack behaviour in naive gyrfalcons is modelled by the same
545 guidance law as in peregrine falcons, but at a lower guidance gain. J Exp Biol. 2021;224.
546 doi:10.1242/jeb.238493

547 30. Kunz TH, Martin RA. *Plecotus townsendii*. Mamm Species. 1982; 1. doi:10.2307/3503998

548 31. Norberg UM, Rayner JMV. Ecological morphology and flight in bats (Mammalia; Chiroptera): wing
549 adaptations, flight performance, foraging strategy and echolocation. Philos Trans R Soc B. 1987;316: 335–
550 427. doi:10.1098/rstb.1987.0030

551 32. Farney J, Fleharty ED. Aspect ratio, loading, wing span, and membrane areas of bats. J Mammal. 1969;50:
552 362–367. doi:10.2307/1378361

553 33. Jones KE, Bielby J, Cardillo M, Fritz SA, O'Dell J, Orme CDL, et al. PanTHERIA: a species-level database of life
554 history, ecology, and geography of extant and recently extinct mammals. Ecology. 2009;90: 2648–2648.
555 doi:10.1890/08-1494.1

556 34. Fellers GM, Pierson ED. Habitat use and foraging behavior of Townsend's big-eared bat (*Corynorhinus*
557 *townsendii*) in coastal California. J Mammal. 2002;83: 167–177. doi:10.1644/1545-
558 1542(2002)083<0167:HUAFBO>2.0.CO;2

559 35. Sherwin RE, Stricklan D, Rogers DS. Roosting affinities of Townsend's big-eared bat (*Corynorhinus*
560 *townsendii*) in northern Utah. J Mammal. 2000;81: 939–947. doi:10.1644/1545-
561 1542(2000)081<0939:RAOTSB>2.0.CO;2

562 36. Hakansson J, Jakobsen L, Hedenström A, Johansson LC. Body lift, drag and power are relatively higher in
563 large-eared than in small-eared bat species. J R Soc Interface. 2017;14: 20170455.
564 doi:10.1098/rsif.2017.0455

565 37. Corcoran AJ, Conner WE. Predator counteradaptations: stealth echolocation overcomes insect sonar-
566 jamming and evasive-manoeuvring defences. Anim Behav. 2017;132: 291–301.
567 doi:10.1016/j.anbehav.2017.08.018

568 38. Hedrick TL. Software techniques for two- and three-dimensional kinematic measurements of biological and
569 biomimetic systems. Bioinspir Biomim. 2008;3: 6. doi:10.1088/1748-3182/3/3/034001

570 39. Theriault DH, Fuller NW, Jackson BE, Bluhm E, Evangelista D, Wu Z, et al. A protocol and calibration method
571 for accurate multi-camera field videography. J Exp Biol. 2014; jeb.100529. doi:10.1242/jeb.100529

572 40. Brighton CH, Thomas ALR, Taylor GK. Terminal attack trajectories of peregrine falcons are described by the
573 proportional navigation guidance law of missiles. Proc Natl Acad Sci U S A. 2017;114: 13495–13500.
574 doi:10.1073/pnas.1714532114

575 41. Kane SA, Fulton AH, Rosenthal LJ. When hawks attack: animal-borne video studies of goshawk pursuit and
576 prey-evasion strategies. J Exp Biol. 2015;218: 212–222. doi:10.1242/jeb.108597

577 42. N.A. Shneydor. Missile guidance and pursuit: kinematics, dynamics and control. Woodhead publishing;
578 1998.

579 43. Fabian ST, Sumner ME, Wardill TJ, Rossoni S, Gonzalez-Bellido PT. Interception by two predatory fly species
580 is explained by a proportional navigation feedback controller. J R Soc Interface. 2018;15.
581 doi:10.1098/rsif.2018.0466

582 44. Ghose K, Moss CF. Steering by hearing: a bat's acoustic gaze is linked to its flight motor output by a
583 delayed, adaptive linear law. J Neurosci. 2006;26: 1704–10. doi:10.1523/JNEUROSCI.4315-05.2006

584 45. Vaughan TA. Morphology and flight characteristics of molossid bats. J Mammal. 1966;47: 249–260.
585 doi:10.2307/1378121

586 46. Domenici P, Blagburn JM, Bacon JP. Animal escapology I: theoretical issues and emerging trends in escape
587 trajectories. J Exp Biol. 2011;214: 2463–73. doi:10.1242/jeb.029652

588 47. Domenici P, Blagburn JM, Bacon JP. Animal escapology II: escape trajectory case studies. J Exp Biol.
589 2011;214: 2474–2494. doi:10.1242/jeb.053801

590 48. Hedenstrom A. Predator versus prey: on aerial hunting and escape strategies in birds. Behav Ecol. 2001;12:
591 150–156. doi:10/d3q96s

592 49. Clemente CJ, Wilson RS. Speed and maneuverability jointly determine escape success: exploring the
593 functional bases of escape performance using simulated games. Behav Ecol. 2016;27: 45–54.
594 doi:10.1093/beheco/arv080

595 50. Moore TY, Cooper KL, Biewener AA, Vasudevan R. Unpredictability of escape trajectory explains predator
596 evasion ability and microhabitat preference of desert rodents. Nat Commun. 2017;8: 1–9.
597 doi:10.1038/s41467-017-00373-2

598 51. Webster FA, Griffin DR. The role of the flight membranes in insect capture by bats. Anim Behav. 1962;10:
599 332–340. doi:10.1016/0003-3472(62)90056-8

600 52. Full RJ, Koditschek DE. Templates and anchors: neuromechanical hypotheses of legged locomotion on land.
601 J Exp Biol. 1999;202: 3325–3332. doi:10.1242/jeb.202.23.3325

602 53. Peterson AN, McHenry MJ. The persistent-predation strategy of the red lionfish (*Pterois volitans*). Proc R
603 Soc B. 2022;289: 20221085. doi:10.1098/rspb.2022.1085

604 54. Soto AP, McHenry MJ. Pursuit predation with intermittent locomotion in zebrafish. J Exp Biol. 2020;
605 jeb.230623. doi:10.1242/jeb.230623

606 55. Denzinger A, Schnitzler H-UU. Bat guilds, a concept to classify the highly diverse foraging and echolocation
607 behaviors of microchiropteran bats. Front Physiol. 2013;4: 1–15. doi:10.3389/fphys.2013.00164

608 56. Dudley R. Mechanisms and implications of animal flight maneuverability. Integr Comp Biol. 2002;42: 135–
609 140. doi:10.1093/icb/42.1.135

610 57. Mizutani A, Chahl JS, Srinivasan MV. Insect behaviour: Motion camouflage in dragonflies. Nature.
611 2003;423: 604. doi:10.1038/423604a

612 58. Pal S. Dynamics of aerial target pursuit. Eur Phys J Spec Top. 2015;224: 3295–3309.
613 doi:10.1140/epjst/e2015-50084-6

614 59. Pais D, Leonard N. Pursuit and evasion: evolutionary dynamics and collective motion. AIAA Guidance,
615 Navigation, and Control Conference. Reston, Virigina: American Institute of Aeronautics and Astronautics;
616 2010. doi:10.2514/6.2010-7584

617 60. Mills R, Hildenbrandt H, Taylor GK, Hemelrijk CK. Physics-based simulations of aerial attacks by peregrine
618 falcons reveal that stooping at high speed maximizes catch success against agile prey. PLoS Comput Biol.
619 2018;14: e1006044. doi:10.1371/journal.pcbi.1006044

620 61. Cowan NJ, Ankarali MM, Dyhr JP, Madhav MS, Roth E, Sefati S, et al. Feedback control as a framework for
621 understanding tradeoffs in biology. Integr Comp Biol. 2014;54: 223–37. doi:10.1093/icb/icu050

622 62. Combes SA, Rundle DE, Iwasaki JM, Crall JD. Linking biomechanics and ecology through predator-prey
623 interactions: flight performance of dragonflies and their prey. J Exp Biol. 2012;215: 903–913.
624 doi:10.1242/jeb.059394

63. Bortoni A, Swartz SM, Vejdani, H, Corcoran, AJ. (2023), [supporting information] Strategic predatory pursuit of the stealthy, highly maneuverable, slow flying bat *Corynorhinus townsendii*, Dryad, Dataset, https://doi.org/10.5061/dryad.05qfttf7j